

Patterning challenges for direct metal etch of ruthenium and molybdenum at 32 nm metal pitch and below

Cite as: J. Vac. Sci. Technol. B **40**, 032802 (2022); <https://doi.org/10.1116/6.0001791>

Submitted: 09 February 2022 • Accepted: 31 March 2022 • Published Online: 26 April 2022

Stefan Decoster, Elisabeth Camerotto, Gayle Murdoch, et al.



View Online




Export Citation




CrossMark





HIDEN
ANALYTICAL



40 YEARS
1982 - 2022


Instruments for Advanced Science

- Knowledge,
- Experience,
- Expertise

Click to view our product catalogue


Contact Hiden Analytical for further details:
www.HidenAnalytical.com
info@hideninc.com

Gas Analysis




- ▶ dynamic measurement of reaction gas streams
- ▶ catalysis and thermal analysis
- ▶ molecular beam studies
- ▶ dissolved species probes
- ▶ fermentation, environmental and ecological studies

Surface Science




- ▶ UHVTPD
- ▶ SIMS
- ▶ end point detection in ion beam etch
- ▶ elemental imaging - surface mapping

Plasma Diagnostics



- ▶ plasma source characterization
- ▶ etch and deposition process reaction kinetic studies
- ▶ analysis of neutral and radical species

Vacuum Analysis



- ▶ partial pressure measurement and control of process gases
- ▶ reactive sputter process control
- ▶ vacuum diagnostics
- ▶ vacuum coating process monitoring

Patterning challenges for direct metal etch of ruthenium and molybdenum at 32 nm metal pitch and below

Cite as: J. Vac. Sci. Technol. B 40, 032802 (2022); doi: 10.1116/6.0001791

Submitted: 9 February 2022 · Accepted: 31 March 2022 ·

Published Online: 26 April 2022



Stefan Decoster,^{1,a)} Elisabeth Camerotto,² Gayle Murdoch,¹ Souvik Kundu,¹ Quoc Toan Le,¹ Zsolt Tőkei,¹ Gosia Jurczak,² and Frédéric Lazzarino¹

AFFILIATIONS

¹IMEC, Kapeldreef 75, 3001 Heverlee, Belgium

²Lam Research Belgium, Kapeldreef 75, 3001 Heverlee, Belgium

^{a)}Electronic mail: stefan.decoester@imec.be

ABSTRACT

Ruthenium and molybdenum are candidate materials to replace Cu as the back-end-of-line interconnect metal for the tightest pitch features for future technology nodes. Due to their better figure of merit $\rho_0 \times \lambda$ (ρ_0 bulk resistivity, λ electron mean free path), it is expected that the resistance of <10 nm wide Ru and Mo metal lines can be significantly reduced compared to Cu. An important advantage for Ru and Mo is that both materials, in contrast to Cu, can be patterned by means of so-called direct metal etch, through reactive ion etching or atomic layer etching and can potentially be implemented without barrier. An integration scheme with direct metal etch instead of damascene patterning could simplify the overall patterning flow and eventually opens the possibility for exploring new integration concepts and patterning approaches. However, the learning on direct metal etch of Ru and Mo in the literature is scarce, especially at the relevant dimensions of today's interconnects. In this work, we will focus on the major patterning challenges we have encountered during the development of direct metal etch processes for Ru at 18 nm pitch and Mo gratings at 32 nm pitch. We have observed that the direct metal etch of Ru at these small dimensions is impacted by the growth of an oxidized layer on the sidewalls of the hard mask, which originates from the sputtering of the hard mask in combination with the O₂-based Ru etch chemistry. This results in a narrowing of the trenches to be patterned and can easily lead to an etch stop in the smallest features. We will discuss several mitigation mechanisms to remove this oxidized layer, as well as to avoid the formation of such a layer. For patterning Mo with a Cl₂/O₂-based chemistry, the major patterning challenges we encountered are the insufficient sidewall passivation and the oxidation of the patterned Mo lines. The sidewall passivation issue has been overcome with an *in situ* thin SiO₂-like deposition after partial Mo etch, while a possible mitigation mechanism for the Mo oxidation could be the *in situ* encapsulation immediately after Mo patterning.

Published under an exclusive license by the AVS. <https://doi.org/10.1116/6.0001791>

I. INTRODUCTION

For several decades, the semiconductor industry has been successfully following Moore's law, which originally stated that the number of transistors in an integrated circuit doubles every two years. This empirical law has been followed by the semiconductor industry through a combination of dimensional scaling, introducing new patterning concepts, innovative device architectures, design-technology co-optimization, tool improvements, and integrating new materials. One of the new materials that was integrated to slow down the increase of the resistive-capacitive (RC) delay for

each technology node in the back end of line (BEOL) in the mid-1990s, was Cu. Because of its lower bulk resistivity and higher electromigration reliability, Cu replaced Al-based interconnects and became the standard material in BEOL interconnects for the last two decades.¹ One of the major technical challenges to replace Al with Cu has been the patterning strategy; while Al and Al-based alloys can be patterned in a direct way by reactive ion etching, the direct metal etch (DME) of Cu has proven to be extremely challenging^{2,3} due to the absence of volatile by-products. Therefore, the DME approach of Al-based interconnects was replaced with the damascene patterning approach, i.e., defining trenches and vias in

a dielectric material, filling these features with a metal, such as Cu, and finally planarizing the structures by a mechanical chemical polishing process.¹ Furthermore, dual damascene processing presented a significant cost advantage over previous methods, as two layers are fabricated in a single step.

Although damascene patterning had to overcome many technical challenges, Cu-based interconnects have been around for many consecutive technology nodes. As we are progressing toward local BEOL interconnect metal pitches of 20 nm and smaller (for technology nodes beyond N2), the resistance of Cu metal lines increases very fast at such small dimensions due to electron scattering at surfaces and at grain boundaries.^{4,5} Moreover, Cu metal lines require a liner to prevent Cu diffusion in the dielectric material. As this liner needs a fixed thickness to prevent diffusion, scaling Cu interconnects without being able to scale the liner thickness results in a significant relative increase in metal resistance as a function of reducing critical dimension. Therefore, many research efforts are currently spent to find alternative metals to replace Cu at these small pitches, both for metal lines as well as for vias.^{5,6}

Two interesting candidates, which are expected to have a lower resistance than Cu at very small dimensions, are ruthenium (Ru) and molybdenum (Mo).⁵ An important advantage for Ru and Mo is that both materials can be patterned by direct metal etch, as was the case with Al before the Cu-interconnect era. Moreover, as both Ru and Mo can be integrated barrierless, a reduction in resistance can be expected when integrating Ru or Mo at small dimensions.^{7–10} Furthermore, DME reduces the overall processing cost by avoiding the costly metallization and chemical mechanical polishing steps in a typical damascene patterning scheme. Finally, the use of DME opens the possibility for exploring new integration concepts and scaling boosters, such as semi-damascene patterning, alternative patterning schemes for self-aligned blocks and vias, hybrid height metal lines, and pillar vias.^{9,11}

It is known for several decades that ruthenium can be patterned with reactive ion etching^{12–17} and even with atomic layer etching¹⁸ in an oxygen-based plasma through the formation of volatile RuO₄, while Ru is very etch-resistant toward halogen-based plasmas. As most of the materials in today's integrated circuits (such as oxides, nitrides, or other metals) cannot be etched in O-based plasmas, integrating Ru as an interconnect metal can be very patterning-friendly. A typical halogen-based hard mask (HM) etch process will not affect Ru, while the O-based Ru etch can be selective to the hard mask as well as to the dielectric layer below Ru, which potentially enables high aspect ratio metal patterning and avoids the use of a dedicated etch stop layer. It should be noted that the DME of Ru does not provide any selectivity to carbon-based layers, such as spin-on carbon, organic photoresist, or amorphous carbon.

Anisotropic etching of Ru has been reported by several groups^{14–16} at relatively relaxed dimensions (>100 nm feature width), while isotropic atomic layer etching of Ru has also been demonstrated.¹⁹ Still, very limited information is available in the literature on anisotropic etching of Ru at the relevant small dimensions, where it could result in a resistance gain when replacing Cu, i.e., at 20 nm metal pitch and below. We have reported earlier on the behavior of anisotropic etching of Ru metal lines at 32 nm pitch^{18,20} and on the electrical outcome and the reliability results of

these features.^{8–10} In the current study, we will share the results of patterning Ru at even smaller dimensions (down to 18 nm metal pitch) on 300 mm wafers and discuss the major patterning challenge encountered during this development, together with a number of mitigation mechanisms to overcome this challenge.

In contrast to Ru, reactive ion etching of molybdenum has been demonstrated in various halogen-based plasma chemistries: fluorine,^{21–26} chlorine,^{21,23,25,27–30} and bromine^{25,30} plasma chemistries have been used to anisotropically etch Mo, albeit at much larger dimensions than targeted in the present study. In the current work, we have chosen to pattern Mo with a chlorine-based chemistry as we can expect an improved selectivity toward the dielectric hard mask, compared to using a fluorine-based chemistry. In the second part of this manuscript, we will present the most important patterning challenges we have faced during the DME of Mo metal lines at 32 nm pitch, and share some learning on potential mitigation options.

II. EXPERIMENT

All the experiments in this study have been performed in Imec's 300 mm cleanroom. An oxide layer was thermally grown on a 300 mm Si substrate wafer, onto which a (Ru or Mo) metal layer was grown.

Due to poor adhesion of Ru on standard dielectric materials such as SiO₂ or Si₃N₄, an adhesion layer of 1 nm TiN was deposited on the bottom oxide layer before the physical vapor deposition (PVD) of Ru. In this study, the deposited thickness of Ru ranged between 20 and 50 nm. After deposition, the wafers have been annealed at 420 °C for 20 min under N₂ atmosphere, to increase the grain size and hence lower the resistivity of the material. After anneal, another thin (1 nm–5 nm) TiN film was deposited to improve the adhesion with the Si₃N₄ hard mask layer.

Molybdenum has been deposited without an adhesion layer below or above the metal layer. A 50 nm thick metal film was grown by means of PVD, without any post-deposition annealing step.

For both metals, we have used Si₃N₄ (denoted as SiN in the remainder of the text), grown by chemical vapor deposition (CVD), as the hard mask. The thickness of the SiN hard mask was varied for Ru and Mo and for different aspect ratios of the patterned metal lines, ranging between 25 and 45 nm. The choice of hard mask is linked to the semi-damascene patterning approach⁹ in which the hard mask of the metal layer is used for the creation of a self-aligned via later in the processing flow. After metal patterning, such self-aligned via can be achieved when there is sufficient etch selectivity between the hard mask material of the metal lines (SiN in our case) and the dielectric material (SiO₂ or low-κ material), which is filled in between the metal lines.

To pattern 32 nm pitch features, we have used an amorphous carbon film on top of the SiN hard mask, followed by the coating of a metal-organic resist. This resist was patterned by means of Extreme Ultraviolet lithography. To pattern features below 32 nm pitch, we have applied a self-aligned double patterning (SADP) scheme, with amorphous Si as the sacrificial mandrel, and SiO₂ as the spacer material. These SiO₂ spacers were then transferred into the SiN hard mask, after which the metal patterning tests could be

performed. Whenever possible, the hard mask etch and the metal etch steps were combined in a single etch process.

All metal etch development presented in this work was done in collaboration with Lam Research and was performed on 300 mm Kiyo® and Versys® tools from Lam Research, both using TCP technology. Full 300 mm wafers have been used for most of the experiments in this study while smaller coupons, extracted from a 300 mm wafer and attached to an SiO₂ carrier wafer, have been used in a few dedicated experiments (Secs. III B 2 and IV A 1). For Ru etch, an O₂-based plasma was used, while Mo was etched in a Cl₂/O₂-based plasma. These etch processes were run at normal pressures (in a 5–50 mTorr range) and at temperatures between room temperature and 120 °C. Small flows of other gases were added to these baseline chemistries to improve the profile, reduce masking, and increase the selectivity towards the hard mask. Further details of these etch processes are not critical for discussing the major patterning challenges to etch Ru and Mo, as presented in this work. It is important to note that the Kiyo® tool was equipped with an *in situ* conformal SiO₂ deposition capability.

Morphological characterization of the metal lines after patterning has been done with cross-sectional scanning electron microscopy (X-SEM) and transmission electron microscopy (TEM). Some of the TEM images have been further investigated with energy dispersive x-ray (EDX) analysis to get additional insights into the chemical composition of the features after metal patterning.

III. RESULTS AND DISCUSSION (1): PATTERNING CHALLENGES FOR RUTHENIUM DME

As mentioned in Sec. I, DME of Ru can be done in an O₂-based plasma.^{12–20} We have used a SiN hard mask with TiN as an adhesion layer between Ru and the hard mask. Under these conditions, we have demonstrated the patterning of 42 nm pitch Ru

metal lines, as shown in Fig. 1(a), with a sidewall angle of 88° with a selectivity of ~8–10 to the hard mask. Interestingly, an additional thin layer on the sides of the SiN hard mask is grown, which can be identified by EDX analysis as an SiO₂-like layer of more than 5 nm, as shown in Figs. 1(b) and 1(c). This mushroom-shaped hard mask will become a major patterning challenge when scaling this direct metal etch process and will be discussed in the next section.

A. Patterning challenge: Oxide growth on the HM sidewalls

While the Ru lines at 42 nm pitch are well-separated from each other, it can be expected that scaling this etch process to smaller pitches will become problematic. The width of the trenches is decreasing due to the build-up of SiO₂ on the sidewalls of the SiN hard mask, which will eventually lead to neighboring features touching each other at the hard mask level. This is shown in Fig. 2, where the Ru metal lines at 32 nm metal pitch (a) can still be patterned well, while the trenches in the case of 21 nm metal pitch gratings (b) are narrowing due to the lateral hard mask growth, resulting in a heavily reduced etch rate in the smaller trenches, or even a complete etch stop. Therefore, we would like to further discuss this behavior as a patterning challenge when etching Ru metal lines at pitches of 32 nm and below. Several mitigation approaches to tackle this patterning challenge will be presented in the following section.

B. Mitigation mechanisms for oxide growth on the HM sidewalls

Several mitigation approaches were investigated to overcome this patterning challenge: (1) cycling between the Ru etch process and an oxide removal step; (2) protecting the HM from the top or from the sidewalls; (3) adding CH_xF_y to the baseline Ru etch chemistry; and (4) adjusting the ion/radical ratio in the Ru etch process to reduce the sputtering of the hard mask material. The learning of these different mitigation mechanisms will be shared below, together with X-SEM and TEM images for patterned Ru lines at 21 nm or 18 nm pitch.

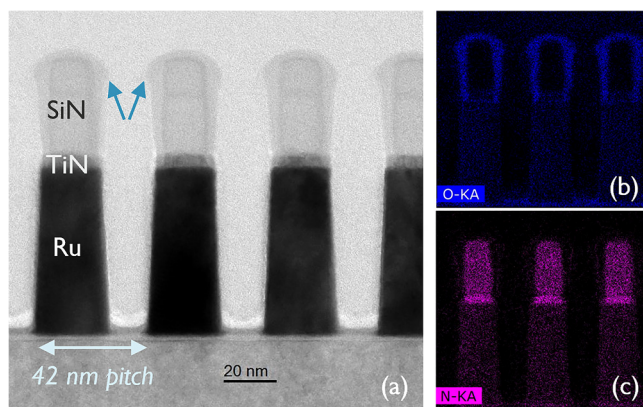


FIG. 1. (a) Cross-sectional TEM image of 42 nm pitch Ru metal lines, with a 5 nm TiN adhesion layer and the remainder of the SiN hard mask on top. EDX analysis for O (b) and N (c) was done on the same image to highlight the presence of an oxidized layer on the outside of the SiN hard mask. Also note that the Ru metal lines do not show any sign of sidewall oxidation.

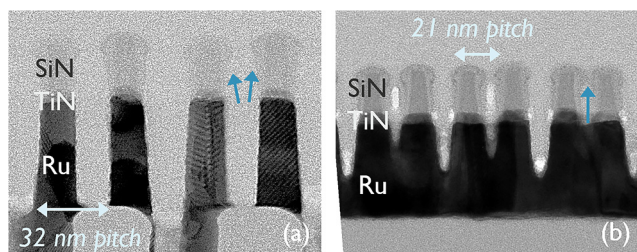


FIG. 2. Cross-sectional TEM images of (a) 32 nm pitch and (b) 21 nm pitch Ru metal lines, with a 5 nm TiN adhesion layer and the remainder of the SiN hard mask on top. The SiO₂ layer is visible on the sidewalls of the SiN hard mask, as indicated by the arrows.

1. Cycling between Ru etch and oxide removal

As a first mitigation mechanism, we applied a cyclic etching process in which one cycle consists of etching ~ 5 nm Ru and removing the oxidized layer on the side of the SiN hard mask by means of a very short fluorocarbon-based isotropic etch process. Several such cycles are repeated until the full Ru metal layer is patterned. As shown in Fig. 3(b), this approach has allowed us to create separated Ru metal lines at 18 nm pitch, although quite some defects can still be observed in between the Ru metal lines.

As there is little etch selectivity between SiO₂ and SiN for a fluorocarbon-based plasma, the time of the oxidation removal step in the cycle is critical: a too short step means that the oxide layer is not fully removed which will lead to trench closing, while a too long removal step will result in extra consumption of the SiN hard mask. As can be seen from Figs. 3(a) and 3(b), 2/3 of the SiN hard mask is lost during the entire process. This indicates that this etching process will not enable higher aspect ratio etching, although this is one of the expected benefits of DME.

2. Protecting the SiN hard mask

An alternative approach to mitigate the growth of the oxidized layer on the SiN hard mask is to protect the SiN during the Ru etch process by covering it with another material. We have tested two different mechanisms, i.e., *sidewall* protection and *top* protection, using two materials for each protection mechanism. The sidewall protection was tested by depositing a thin (~ 1 nm) conformal layer of SiO₂ or Al₂O₃ on the already patterned SiN hard mask. Next, the top and bottom part of this conformal layer are etched back, resulting in a thin protection layer on the sidewalls of the SiN hard mask. Creating a top protection layer was performed by adding a 5 nm thin layer of TiN or Al₂O₃ in the patterning stack on top of the SiN hard mask, before defining the gratings or opening the hard mask. This layer was then patterned together with the SiN hard mask, which results in a thin protection layer on top of the SiN.

These different protection mechanisms are schematically represented in Figs. 4(a)–4(d), together with Figs. 4(e)–4(h) X-SEM images after hard mask opening and (i)–(l) after Ru patterning. All tests were carried out with a line/space grating at 21 nm pitch, but with slightly different Ru metal and SiN hard mask thickness.

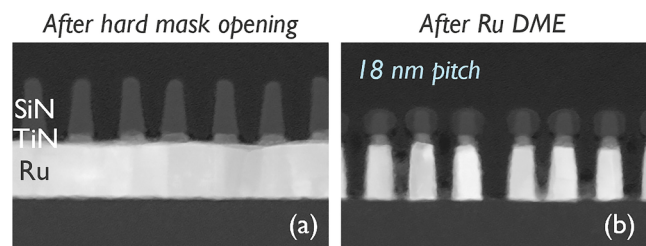


FIG. 3. Cross-sectional TEM images of 18 nm pitch gratings (a) after SiN/TiN hard mask opening and (b) after Ru direct metal etch, where a cyclic process was used, alternating between etching Ru and removing the oxidized layer with a short fluorocarbon-based etch step.

When protecting the *sidewalls* of the SiN hard mask with a thin layer of SiO₂ [Fig. 4(e)], we clearly observe a lateral growth of the hard mask after the direct metal etch of Ru [Fig. 4(i)], resulting in a closing of the trenches. The same behavior is observed when protecting the hard mask with a thin layer of Al₂O₃ [Fig. 4(f)]: although the trenches are not entirely closed, the hard mask has increased by ~ 4 nm in width after patterning the Ru metal lines [Fig. 4(j)]. Even though both SiO₂ and Al₂O₃ are expected to be inert in an O₂-based plasma, both test results indicate that protecting the sidewalls of the SiN hard mask with either of these two materials is unsuccessful in preventing a lateral growth of the hard mask.

The results of the second protection mechanism, i.e., protecting the SiN hard mask from the *top* before Ru direct metal etch, are shown in Fig. 4(k) for adding 5 nm of TiN. When comparing the results after Ru patterning to the same samples after hard mask patterning [Fig. 4(g)], we observe an increase of ~ 4 nm in the hard mask width, while the Ru layer is not yet fully etched. Finally, adding 5 nm of Al₂O₃ on top of the SiN layer results in a more promising behavior [Fig. 4(l)]. The hard mask does not significantly increase in width compared to the image after hard mask opening [Fig. 4(h)], while the Ru metal lines have been fully etched.

To summarize the results in this section, we can conclude that the sidewall protection of the hard mask does not prevent the hard mask to grow laterally, while the top protection of the SiN hard mask was only successful in the case of an Al₂O₃ layer, but not for TiN. These results indicate that the growth of the oxide-rich layer on the sidewall of the SiN hard mask is only inhibited when there is no Si (or Ti-atoms) exposed from the top during the Ru etch process. This leads us to believe that the increase in the SiN hard mask width is not related to the oxidation of the hard mask, but rather to the sputtering of the hard mask, followed by redeposition and oxidation (due to the O-plasma) of the sputtered atoms. Al₂O₃ is expected to have a relatively low chemical sputtering rate, although we cannot exclude the possibility that some Al atoms are being physically sputtered. Still, Fig. 4(l) shows that there is no or very limited redeposition taking place when the SiN HM is protected with Al₂O₃ from the top. This indicates that very little sputtering is occurring, and that the sputtered atoms (Al) are less likely to stick to the walls of the SiN HM.

On the other hand, when SiN (or TiN) is exposed during the Ru etch, sputtering and redeposition of Si or Ti atoms from the top of the SiN hard mask or from the top TiN layer, followed by oxidation from the oxygen radicals in the Ru etch plasma could explain the growth of SiO₂-like or TiO₂-like material on the sidewalls of SiN.

Although the protection of the SiN layer with a thin Al₂O₃ layer shows some potential, integrating an Al₂O₃ layer in the hard mask stack is not a straightforward task at these small dimensions and is a potential cause of extra defects. These experiments have been performed to understand the mechanism of the growth of the hard mask, rather than to suggest that this stack is a good candidate for the direct metal etch of Ru at these small dimensions.

3. Addition of CH_xF_y to the Ru etch chemistry

As a third approach to avoid the growth of an oxide-rich layer on the sidewalls of the SiN hard mask, we have added a small fraction (less than 5% of the total gas flow) of CH_xF_y to the O₂-based plasma chemistry. The main goal is to enable the formation of

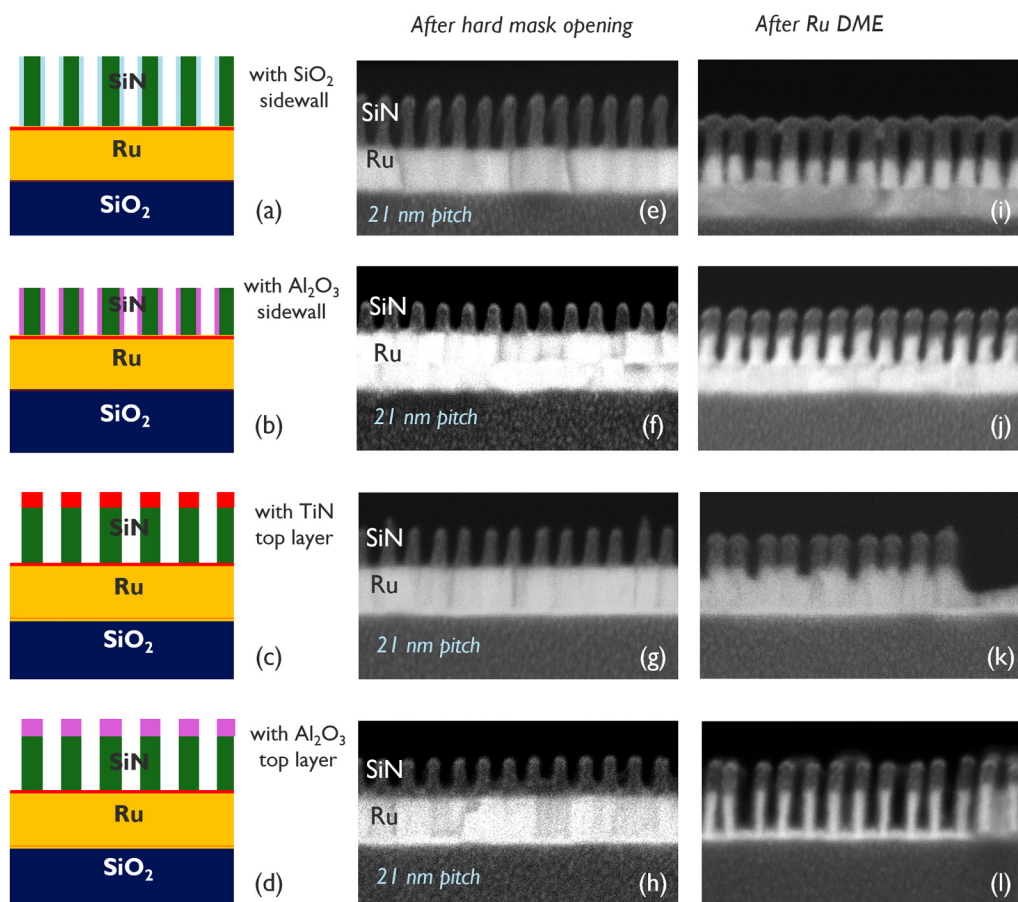


FIG. 4. (a)–(d) Schematic representations and XEM images [(e)–(h)] after hard mask opening and [(i)–(l)] after DME of Ru for 21 nm pitch gratings with different hard mask protection mechanisms: [(a), (e), and (i)] a 1 nm SiO_2 and [(b), (f), and (j)] a 1 nm Al_2O_3 protection layer on the sidewalls of the hard mask, [(c), (g), and (k)] a 5 nm TiN and [(d), (h), and (l)] a 5 nm Al_2O_3 protection layer on top of the SiN hard mask.

volatile by-products for the sputtered Si atoms and hence to avoid the redeposition of the sputtered Si atoms and the growth of the SiN hard mask. In Fig. 5, we present the results of a 21 nm pitch line/space grating (a) after hard mask opening, (b) after etching the Ru metal lines with the baseline Ru etch chemistry and (c) with CH_xF_y addition to the baseline. As can be noticed by the experienced eye, the addition of CH_xF_y results in a straighter hard mask profile compared to the baseline chemistry where a mushroom-like shape of the hard mask becomes apparent. Moreover, when adding CH_xF_y , the so-called field area (which is the large open area next to the dense features) is etched in a more equal way, compared to the baseline chemistry. Without the addition of CH_xF_y , a masking behavior is obvious [Fig. 5(b)], which can be removed by substantial over-etching.

The observations from Fig. 5 coincide with the hypothesis of sputtered Si atoms from the SiN hard mask during the Ru etch process. When CH_xF_y is added to the baseline Ru etch gas mixture, volatile by-products can be formed for the sputtered Si atoms,

which avoids the redeposition of these atoms on the sidewalls and the growth of the SiN hard mask. Moreover, the masking behavior on the field [as seen in Fig. 5(b)] can also be attributed to sputtered Si atoms being redeposited on the field and hence masking the Ru etch below. When adding CH_xF_y to the baseline chemistry, this masking behavior is not observed anymore.

These results indicate that adding CH_xF_y to the O-based chemistry is a promising approach to mitigate the growth of the hard mask and the narrowing of the trenches during the Ru direct metal etch. On the downside, however, an increased hard mask consumption is expected when adding CH_xF_y , as can be observed in Figs. 5(b) and 5(c).

4. Reducing the ion/radical ratio to avoid hard mask sputtering

The last mitigation mechanism we have investigated in this study, to avoid the growth of the SiN hard mask during the direct

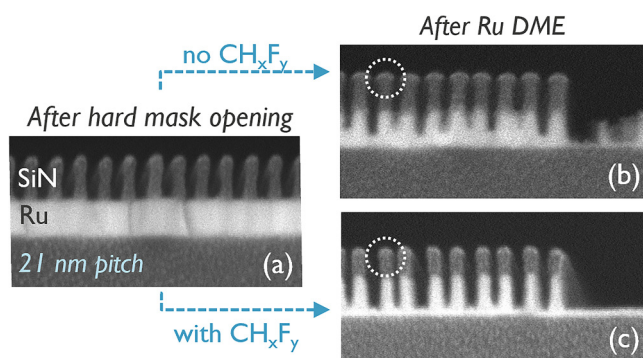


FIG. 5. X-SEM images after (a) hard mask opening and (b) after direct metal etch of Ru lines at 21 nm pitch with the baseline O₂-based Ru etch chemistry and (c) with addition of a small fraction (<5%) of CH_xF_y to the baseline. The dotted circles in (b) and (c) are highlighting the difference in the hard mask shape between both tests.

metal etch of Ru lines, is reducing the ion/radical ratio during the Ru etch process. By significantly reducing the number of ions, while keeping a similar number of radicals, we target to reduce the sputtering of the hard mask, and hence to lower the number of sputtered Si atoms that could redeposit on the SiN hard mask. This reduction in ion/radical ratio was obtained by halving the TCP power and doubling the pressure during the Ru etch, without significantly affecting the Ru etch rate.

In Fig. 6, we present TEM images of 18 nm pitch Ru metal lines patterned with the different Ru etch processes, as described earlier with (a) a cyclic process of Ru etch and oxide removal, and (b) the addition of CH_xF_y to the Ru etch chemistry. As can be seen from Fig. 6(c), reducing the number of ions in the Ru etch process reduces the sputtering and the redeposition of the hard mask, compared to the cyclic process where Ru etch and oxide removal steps are alternated [Fig. 6(a)] or when CH_xF_y is added to the Ru etch chemistry [Fig. 6(b)]. This can be seen from the

thinner oxide layer on the side of the SiN hard mask, as well as from the increased remaining hard mask height. As such, the selectivity to the SiN hard mask has been increased to more than 5:1. It should be noted that the results shown in Fig. 6(c) are a combination of reducing the number of ions with the addition of CH_xF_y to the Ru etch chemistry. Therefore, at the same time, the clearing of the field area is improved, as well as volatile by-products are created for the few sputtered atoms originating from the SiN hard mask.

In summary, we have tested different mitigation mechanisms to avoid the growth of the SiN hard mask during the direct metal etch process of Ru with an O₂-based chemistry. All previously shared results corroborate the hypothesis that the sputtering of the SiN hard mask is at the origin of the increase of the SiN hard mask width. Therefore, by creating volatile by-products for the sputtered atoms (by adding CH_xF_y) and at the same time reducing the number of sputtered atoms (by lowering the ion/radical ratio in the plasma), we can avoid the narrowing of the trenches. At the same time, we obtain a higher hard mask selectivity, which enables to pattern Ru metal lines with a higher aspect ratio.

C. Best known process of Ru DME at 18 nm pitch

The current best process for Ru DME is a combination of the two latter mitigation approaches, i.e., adding CH_xF_y to the baseline chemistry and significantly reducing the ion/radical ratio. This has enabled the patterning of 18 nm pitch Ru metal lines with an aspect ratio (AR) up to three. As shown in Fig. 7(a) for AR 2 and in Fig. 7(b) for AR 3, there is sufficient hard mask remaining to pattern Ru metal lines with an even higher aspect ratio. The metal lines have a straight profile (~90°) and a width of ~11 nm.

These results have been obtained on 300 mm wafers. The Ru etch process is uniform across the wafer, as can be observed from Fig. 8 where images are shown for 18 nm pitch Ru lines with an aspect ratio of 2.5 from (a) the center, (b) halfway between the center and the edge, and (c) the edge of the wafer. The amount of

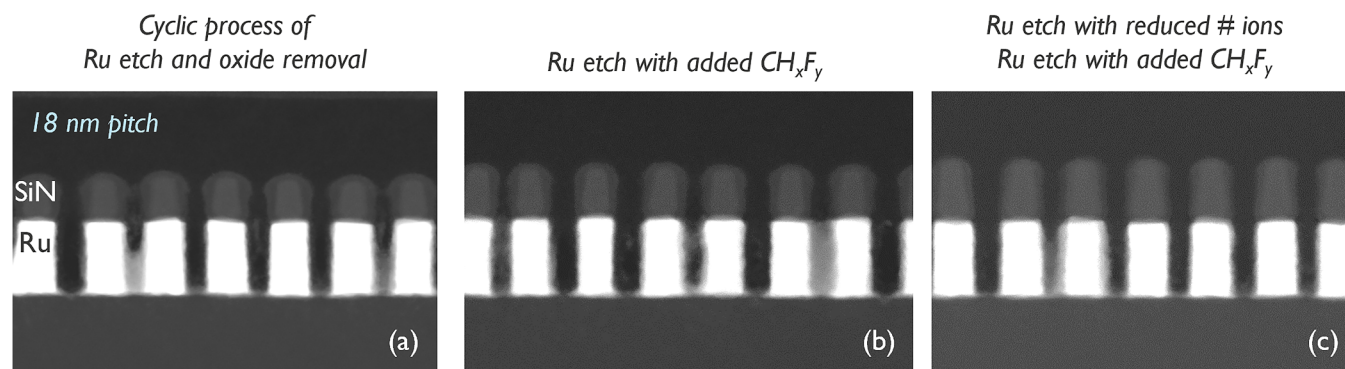


FIG. 6. Cross-sectional TEM images of patterned Ru metal lines at 18 nm pitch (a) with a cyclic process which alternates between Ru etch and removal of the oxidation of the SiN hard mask, (b) with a Ru etch process with addition of CH_xF_y, and (c) with a Ru etch process with both the addition of CH_xF_y and a significantly reduced ratio of ions vs. radicals.

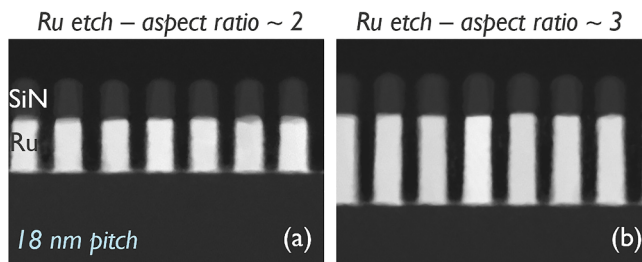


FIG. 7. Cross-sectional TEM images of patterned Ru metal lines at 18 nm pitch with our current best known process, with the addition of CH_3F_y to the etch chemistry and a reduced ion/radical ratio. Results are shown for aspect ratio 2 (a) and 3 (b).

hard mask remaining across the wafer only varies by ~ 1 nm, while the difference in the width of the metal lines across the wafer is well below 1 nm. Some pitch-walking is observed toward the edge of the wafer, which is not related to the Ru etch process itself but can be adjusted by tuning the mandrel width uniformity during the first steps of the SADP process.

IV. RESULTS AND DISCUSSION (2): PATTERNING CHALLENGES FOR MOLYBDENUM DME

In contrast to Ru, molybdenum can be patterned anisotropically in halogen-based chemistries but is not etchable in O-based plasmas. To ensure a high enough selectivity toward the dielectric (SiN) hard mask, we chose a Cl_2 -based chemistry to pattern Mo. By adding O_2 to the plasma, we targeted to enable the formation of volatile MoO_xCl_y by-products.

In this section, we share the learning from the direct metal etch study of Mo metal lines at 32 nm pitch and discuss the two major patterning challenges in combination with a possible mitigation strategy. First, in Sec. IV A the sidewall passivation of the Mo metal lines will be discussed, followed in Sec. IV B by the oxidation of the Mo metal lines.

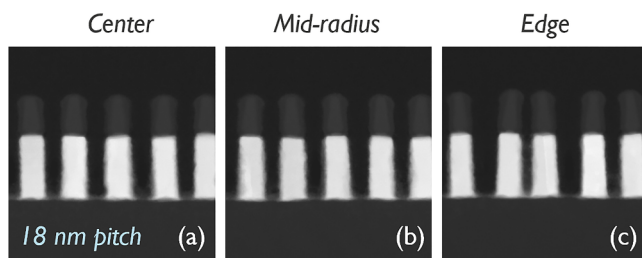


FIG. 8. Cross-sectional TEM images of patterned Ru metal lines at 18 nm pitch with aspect ratio of 2.5, processed with our best known Ru direct metal etch process on a 300 mm wafer. Images are presented from (a) the center, (b) halfway between center and edge, and (c) the edge of the wafer, indicating good uniformity across wafer for the Ru etch process.

A. Patterning challenge 1: Sidewall passivation

1. Patterning results

As shown in Fig. 9(a), we have used a SiN hard mask to pattern Mo. To increase the hard mask budget, the amorphous carbon layer, used as a mask to pattern the SiN layer, was not stripped before the direct metal etch of Mo. All patterning tests shared in this study were performed on 40–50 nm thick Mo films, using a 32 nm pitch hard mask grating. After partial Mo etch [Fig. 9(b)] with the baseline Cl_2/O_2 plasma process, a clear etch loading effect is observed: the field area is fully etched, while the dense line/space grating is only partially etched into the Mo layer. After over-etching with a similar etch chemistry [Fig. 9(c)], a tapered profile of the Mo metal lines is observed, in combination with poor hard mask selectivity and a lateral attack of the top part of the Mo lines. While the tapered profile could possibly be mitigated by over-etching longer, this would entirely remove the hard mask and result in even more lateral attack of the top part of the Mo lines. This latter behavior is linked to an insufficient passivation of the Mo sidewalls, resulting in a chemical lateral attack of the Mo lines during over-etching.

Since a well-tuned sidewall passivation is crucial for obtaining a straight profile, a lot of efforts have been spent on tuning the Cl_2/O_2 -based chemistry during the over-etch step to improve the sidewall passivation and consequently the profile after Mo direct metal etch. A possible passivation mechanism is the creation of a MoO_x -rich sidewall layer, as this was found to inhibit the formation

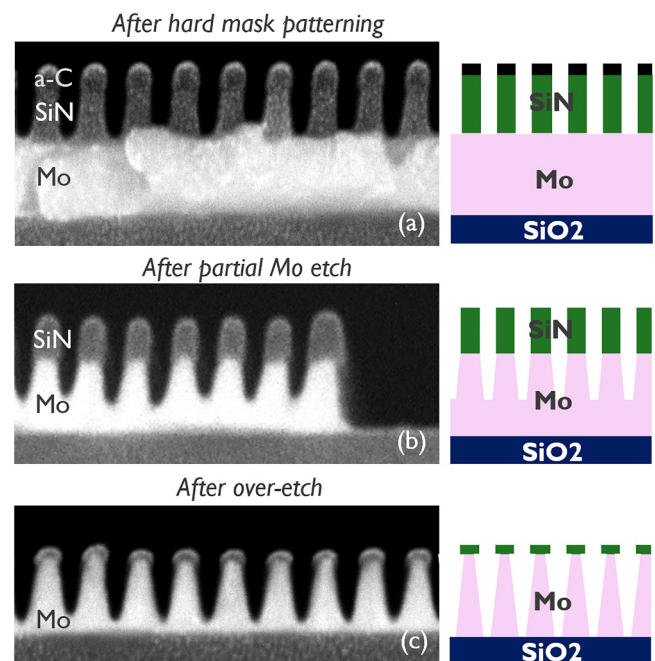


FIG. 9. (Left) X-SEM images and (right) a schematic representation of 32 nm pitch gratings (a) after a-C/SiN hard mask patterning, (b) after partial etch into the Mo layer and (c) after over-etch. The Mo lines are tapered, there is poor hard mask selectivity and a lateral attack of the top part of the Mo lines is observed.

of volatile MoO_xCl_y species.²⁵ Figure 10 consists of a selection of X-SEM images of patterned Mo lines with the same partial Mo etch process as shown in Fig. 9(b), but with different over-etch conditions. As can be seen from Figs. 10(a)–10(h), despite numerous efforts and tuning different process parameters, the profiles of the Mo lines for all the applied experimental conditions are very similar, i.e., tapered with an average sidewall angle of 80° and with lateral attack of 4–6 nm on each side of the top part of the Mo line.

Although not shown here, it is worth mentioning that similar sidewall passivation difficulties were encountered when using a Br-based plasma. When using a F-based plasma to etch Mo, the hard mask selectivity was too poor to etch the entire Mo layer. Therefore, our focus was kept on the direct metal etch of Mo with a Cl_2/O_2 -based plasma.

2. Mitigation mechanism

A solution for the sidewall passivation challenge was found in the *in situ* deposition functionality of the Lam Kiyo® tool. This feature enables the deposition of a conformal SiO_2 -like layer with a very accurate thickness control *in situ* in the etch chamber. This deposition process can be done before, in between or after the etch process. We have deposited a ~ 1 nm thin SiO_2 -like layer *in situ*, immediately after the partial Mo etch [Fig. 9(b)], followed with a Mo over-etch step. This SiO_2 -like layer acts as the passivation layer at the top of the Mo line, which allows us to perform a long

enough over-etch to straighten up the profile at the bottom, without laterally attacking the top part of the Mo lines.

The result of this entire process sequence, i.e., partial etch followed by an *in situ* deposition and a Mo over-etch step, is shown in the X-SEM image in Fig. 11(a). As can be seen from comparing this X-SEM image with all the images from Fig. 10, the Mo profile has been substantially improved, reaching a sidewall angle of $\sim 87^\circ$. Elemental EDX analysis of a TEM image of this improved process [Fig. 11(b)] is shown in Figs. 11(c)–11(f), for Mo, N, Si, and O, respectively. While the shape of the Mo metal line and the SiN hard mask can be clearly deduced from Figs. 11(c) and 11(d), the *in situ* deposited passivation layer is well detectable from the Si signal in Fig. 11(e), as highlighted by the arrow. As expected, the Si signal from the passivation layer stops halfway the Mo metal line, as we only deposited the SiO_2 -like layer after partial etch of the dense Mo lines.

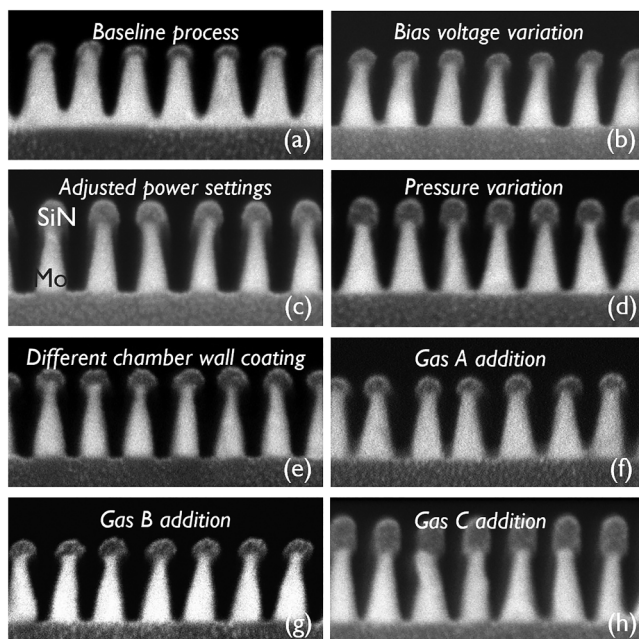


FIG. 10. X-SEM images of patterned Mo lines at 32 nm pitch, with the same partial Mo etch starting condition [Fig. 9(b)], but with different over-etch conditions [(a)–(h)], as specified on top of each image. All process conditions demonstrate insufficient sidewall passivation, as is evidenced from the small width at the top of the Mo lines.

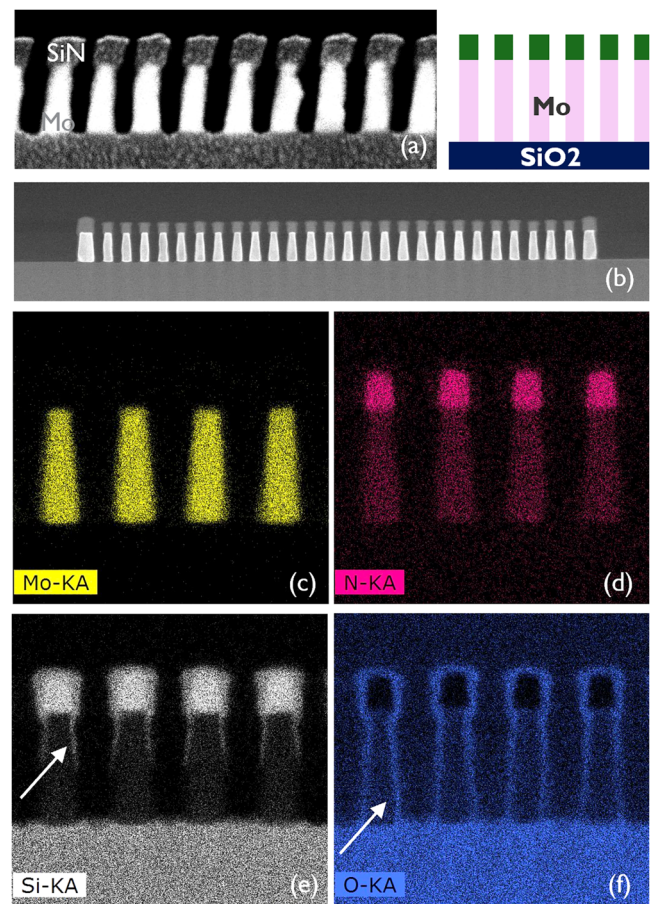


FIG. 11. (a) X-SEM image and schematic representation of patterned Mo lines at 32 nm pitch, by using an *in situ* SiO_2 deposition after the partial Mo etch, followed by an over-etch step. (b) Cross-sectional TEM image of the same process and (c)–(f) elemental analysis of the TEM image from EDX for (c) Mo, (d) N, (e) Si and (f) O. The arrows in (e) and (f) indicate the deposited SiO_2 sidewall passivation layer and the oxidized sidewall of the Mo line, respectively.

From the O signal in Fig. 11(f), an SiO₂-like layer on the sides of the SiN hard mask can be noticed, as well as the presence of the SiO₂ passivation layer at the top of the Mo line. More interestingly, however, is the clear O signal present on the sidewalls at the bottom of the Mo metal line. This oxidation of the metal is not observed when doing direct metal etch of Ru [see Fig. 1(b)] and will likely result in a resistance penalty for patterned Mo lines due to the presence of an oxidized (and hence less conductive) sidewall. This metal oxidation is the second patterning challenge for the direct metal etch of Mo and will be further discussed in the next section.

B. Patterning challenge 2: Metal oxidation

1. Blanket Mo oxidation tests

The O-signal from the EDX analysis on the TEM image after the patterning of Mo lines at 32 nm pitch [Fig. 11(f)] clearly proves that the metal lines are oxidized. The origin of this oxidation is, however, not entirely clear yet. Therefore, we have performed blanket wafer tests to check the presence and quantify the thickness of the MoOx surface layer under different processing conditions. The thickness of the MoOx layer was determined from TEM images in combination with EDX analysis. An example of such TEM images is shown in Fig. 12(a), with corresponding elemental composition maps for Si, O, and Mo in Figs. 12(b)–12(d). A graph with the measured MoOx thickness for each process condition is shown in Fig. 12(e).

As a reference process, we inspected a wafer with an as-deposited Mo layer without any further processing steps. The thickness of the MoOx layer on this wafer was found to be surprisingly thick, i.e., ~3.5 nm. This indicates that Mo needs to be treated very carefully to avoid spontaneous oxidation after deposition.

To verify whether the gas composition of the plasma etch chemistry during the direct metal etch of Mo is playing a role, we exposed a wafer with the baseline Cl₂/O₂ plasma and one with an O₂-free Cl₂ plasma. The measured MoOx thickness was ~3 nm for both wafers, which indicates that the air exposure of the Mo layer after plasma treatment conceals any learning of the possible impact of the O₂-presence in the plasma chemistry of the direct metal etch process. Finally, we tested whether the MoOx layer can be removed with a post-patterning wet cleaning step, using three different cleaning solutions. While one of these cleaning solutions was reducing the measured MoOx thickness after air exposure from ~3 nm to ~2 nm, none of these solutions were able to fully remove and at the same time inhibit the formation of an oxidized Mo surface layer.

Based on these experiments and under the tested conditions, we can expect to have ~2 nm of MoOx sidewalls on the Mo metal lines, patterned with our direct metal etch process. For a 16 nm metal line (for 32 nm pitch gratings), this means that ~4 nm of the metal line width is converted into MoOx, which increases the resistance of the Mo line with ~30% compared to a pure metallic Mo line. For 20 nm pitch gratings and 10 nm Mo lines, this could result in a resistance penalty of more than 60%, which could be a major showstopper for integrating Mo in the future interconnects.

2. Mitigation mechanism: Encapsulation

We have observed that the oxidation of Mo happens spontaneously on an as-deposited film, after patterning and even after

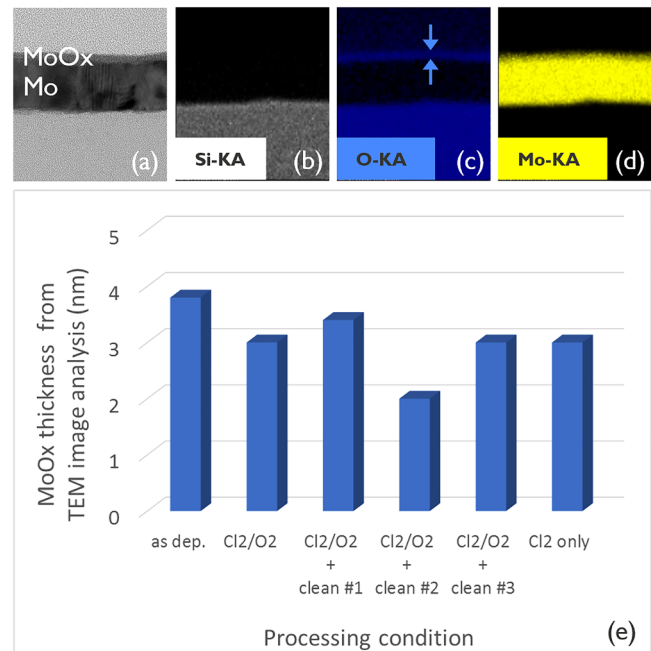


FIG. 12. (a) Cross-sectional TEM image of a blanket Mo film, complemented with EDX analysis for (b) Si, (c) O, and (d) Mo to determine the elemental composition of the TEM image. (e) The extracted MoOx thickness from TEM/EDX analysis for the blanket Mo films, as deposited (as dep.), exposed to the baseline Mo etch chemistry (Cl₂/O₂) or to an O₂-free Mo etch chemistry (Cl₂ only), and treated with different wet clean processes.

different wet clean treatments. Based on these results, the only possible mitigation approach we currently envision is the encapsulation of the Mo metal lines, *in situ* and immediately after patterning. Such a deposition process should be ideally O₂-free and should become a barrier for the oxidation of the Mo lines. To avoid a major penalty in capacitance, this encapsulation layer should also have a relatively low κ value. Defining the proper material and deposition technique that meets all these requirements will be an important challenge to enable the integration of tight pitch Mo metal lines by means of direct metal etch.

V. SUMMARY AND CONCLUSIONS

In summary, we have discussed the major patterning challenges we encountered during the development of direct metal etch processes for ruthenium and molybdenum metal lines at 18 and 32 nm pitch, respectively, on 300 mm wafers. We have also presented mitigation mechanisms to overcome these patterning challenges.

An important patterning challenge during the direct metal etch of Ru is the unwanted growth of an oxide-like layer on the sidewalls of the SiN hard mask, which results in a narrowing of the trenches and prevents a straight Ru metal etch at the smallest trenches. We have presented different mitigation mechanisms to avoid this growth on the sidewalls of the SiN hard mask. The most successful mitigation approaches were the protection of the SiN

hard mask from the top with a thin Al_2O_3 layer, the addition of CH_3F_y to the Ru etch chemistry and reducing the ion/radical ratio of the Ru etch plasma. From these results, we believe that the origin of this growth on the sidewalls of the SiN hard mask can be linked to the sputtering of the SiN hard mask, followed by redeposition and oxidation (from the O_2 -based plasma) of these sputtered species. Hence, by reducing the sputtering of the hard mask, we have avoided the narrowing of the trenches during Ru direct metal etch and enabled the patterning of Ru metal lines at 18 nm pitch with an aspect ratio of 3. We have achieved a vertical profile ($\sim 90^\circ$ sidewall angle) and a hard mask selectivity above 5:1, which enables a further increase in the aspect ratio of the patterned Ru lines.

We have encountered two major patterning challenges during the DME of 32 nm pitch Mo lines using a Cl_2/O_2 -based chemistry. The first challenge was the tapered profile of the Mo lines and the lateral attack of the top of the Mo lines during the over-etch process, caused by a lack of sufficient sidewall passivation. This patterning challenge was mitigated by depositing *in situ* a ~ 1 nm thin SiO_2 -like layer after the partial etch of the Mo lines, followed by a final over-etch step.

The second patterning challenge we have discussed for the DME of Mo is the spontaneous oxidation of the metal lines. From blanket Mo experiments, we observed a 2–3 nm thick MoO_x layer on an as-deposited film, as well as under different plasma etch chemistries and wet treatments. To mitigate this oxidation behavior, an *in situ* O_2 -free encapsulation process of a low κ material, immediately after patterning the Mo lines would be required.

As a final summary, we would like to draw a comparison between the direct metal etch of Ru and Mo, targeting sub-20 nm pitch gratings. As can be deduced from the present work, patterning Ru metal lines can currently be achieved at a much tighter pitch (18 nm pitch) than Mo (32 nm pitch). One of the reasons for this is the challenging sidewall passivation and hence difficult profile control for Mo at smaller pitches, while smooth and nearly vertical profiles can be achieved for Ru. Moreover, the patterned Ru lines do not show any sign of oxidation, while a spontaneous oxidation is observed for Mo. This will result in a significant resistance penalty for Mo, which will be even worse at smaller dimensions. Finally, to reach high aspect ratio metal lines at very tight pitch, the selectivity toward the hard mask will be crucial. Again, Ru DME seems to be more promising than Mo due to the use of O_2 -based plasma, which has the potential to reach an excellent selectivity toward many possible hard mask materials.

ACKNOWLEDGMENTS

Imec has received funding from the ECSEL Joint Undertaking (JU) under Grant Agreement No. 875999. The JU receives support from the European Union's Horizon 2020 research and innovation program and the Netherlands, Belgium, Germany, France, Austria, Hungary, United Kingdom, Romania, and Israel. Furthermore, we gratefully acknowledge the 300 mm Fab operations team at imec for their support, the thin films team for the growth of the metal layers, the X-SEM and TEM (EDX) metrology teams for providing high quality images and the colleagues at imec and at Lam Research for numerous discussions and much-appreciated feedback.

AUTHOR DECLARATIONS

Conflict of Interest

The authors have no conflicts to disclose.

DATA AVAILABILITY

The data that support the findings of this study are available from the corresponding author upon reasonable request.

REFERENCES

- Y. L. Cheng, C. Y. Lee, and Y. L. Huang, "Copper metal for semiconductor interconnects," in *Noble and Precious Metals-Properties, Nanoscale Effects and Applications* (Intechopen, London, 2018), Chap. 10.
- L. Wen *et al.*, in *IEEE IITC and 2015 IEEE MAM Conference* (IEEE, Grenoble, 2015), pp. 173–176.
- F. Wu, G. Levitin, and D. W. Hess, *ACS Appl. Mater. Interfaces* **2**, 2175 (2010).
- P. Kapur, J. P. McVittie, and K. C. Saraswat, *IEEE Trans. Electron Devices* **49**, 590 (2002).
- D. Gall, *J. Appl. Phys.* **127**, 050901 (2020).
- M. H. Van der Veen *et al.*, in *IEEE IITC Conference* (IEEE, Santa Clara, 2018), pp. 172–174.
- S. Dutta *et al.*, *IEEE Electron Device Lett.* **38**, 949 (2017).
- D. Wan *et al.*, *IEEE International Interconnect Technology Conference* (IEEE, Santa Clara, 2018), pp. 10–12.
- G. Murdoch, Z. Tokei, S. Paolillo, O. V. Pedreira, K. Vanstreels, and C. J. Wilson, *IEEE International Interconnect Technology Conference* (IEEE, San Jose, 2020), pp. 4–6.
- A. Lesniewska *et al.*, *IEEE International Reliability Physics Symposium* (IEEE, Monterey, 2021), pp. 1–6.
- Z. Tokei *et al.*, in *IEEE International Electron Devices Meeting 32.2.1-4* (IEEE, San Francisco, 2020).
- W. E. Bell and M. Tagami, *J. Phys. Chem.* **67**, 2432 (1963).
- W. Pan and S. B. Desu, *J. Vac. Sci. Technol. B* **12**, 3208 (1994).
- T. Yunogami and K. Nojiri, *J. Vac. Sci. Technol. B* **18**, 1911 (2000).
- H. W. Kim, J.-H. Han, B.-S. Ju, C.-J. Kang, and J.-T. Moon, *Mater. Sci. Eng. B* **95**, 249 (2002).
- H. W. Kim, B.-S. Ju, and C.-J. Kang, *Microelectron. Eng.* **65**, 319 (2003).
- C. C. Hsu, J. W. Coburn, and D. B. Graves, *J. Vac. Sci. Technol. A* **24**, 1 (2006).
- S. Tan *et al.*, "Atomic layer etch-Advancing its application with a new regime," in *Invited Talk at 6th International Atomic Layer Etching Workshop* (ALE, Bellevue, 2019).
- Y. Gong and R. Akolkar, *J. Electrochem. Soc.* **167**, 062510 (2020).
- S. Paolillo, D. Wan, F. Lazzarino, N. Rassoul, D. Piumi, and Z. Tokei, *J. Vac. Sci. Technol. B* **36**, 03E103 (2018).
- T. P. Chow and A. J. Steckl, *J. Electrochem. Soc.* **131**, 2325 (1984).
- A. Picard and G. Turban, *Plasma Chem. Plasma* **5**, 333 (1985).
- R. J. Saia and B. Gorowitz, *J. Electrochem. Soc.* **135**, 2795 (1988).
- B. W. Smith, C. Fonseca, L. Zavyalova, Z. Alam, and A. Bourov, *J. Vac. Sci. Technol. B* **15**, 2259 (1997).
- O. Luere, E. Pargon, L. Vallier, and O. Joubert, *J. Vac. Sci. Technol. B* **29**, 011024 (2011).
- L. Maduro, C. de Boer, M. Zuiddam, E. Memisevic, and S. Conesa-Boj, *Phys. E* **134**, 114903 (2021).
- Y. Kurogi and K. Kamimura, *Jpn. J. App. Phys.* **21**, 168 (1982).
- S. Franssila, *J. Vac. Sci. Technol. B* **12**, 2963 (1994).
- D. Ha, H. Takeuchi, Y.-K. Choi, and T.-J. King, *IEEE Trans. Electron Dev.* **51**, 1989 (2004).
- V. Paraschiv, W. Boullart, and E. Altamirano-Sanchez, *Microelectron. Eng.* **105**, 60 (2013).